Paleoceanography and Paleoclimatology®

RESEARCH ARTICLE
10.1029/2024PA004997

Contraction of the Western Pacific Tropical Rain Belt and Weakening of the Walker Circulation: Future Lessons From the Past Two Interglacials

S. C. Bova[1], **Y. Rosenthal**[2,3], **and X. Du**[4]

[1]Department of Earth and Environmental Sciences, San Diego State University, San Diego, CA, USA, [2]Department of Marine and Coastal Sciences, Rutgers University, New Brunswick, NJ, USA, [3]Department of Earth and Planetary Sciences, Rutgers University, New Brunswick, NJ, USA, [4]Department of Atmospheric, Oceanic, and Earth Sciences, George Mason University, Fairfax, VA, USA

Key Points:

- Precession driven expansion and contraction dominates variability in the Western Pacific tropical rain band in the last two interglacials
- Modes of variability and rainfall intensity are insensitive to the amplitude of seasonal insolation change
- Heightened sensitivity of the Pacific Walker Circulation to greenhouse gases and sea level under low boreal fall insolation

Supporting Information:

Supporting Information may be found in the online version of this article.

Correspondence to:

S. C. Bova,
sbova@sdsu.edu

Citation:

Bova, S. C., Rosenthal, Y., & Du, X. (2025). Contraction of the Western Pacific tropical rain belt and weakening of the Walker Circulation: Future lessons from the past two interglacials. *Paleoceanography and Paleoclimatology*, *40*, e2024PA004997. https://doi.org/10.1029/2024PA004997

Received 14 AUG 2024
Accepted 21 MAR 2025

Author Contributions:

Conceptualization: S. C. Bova, Y. Rosenthal
Data curation: S. C. Bova
Formal analysis: S. C. Bova, X. Du
Funding acquisition: S. C. Bova, Y. Rosenthal, X. Du
Investigation: S. C. Bova, Y. Rosenthal, X. Du
Methodology: S. C. Bova
Project administration: S. C. Bova
Resources: S. C. Bova, Y. Rosenthal
Supervision: Y. Rosenthal
Visualization: S. C. Bova, X. Du
Writing – original draft: S. C. Bova
Writing – review & editing: S. C. Bova, Y. Rosenthal, X. Du

Abstract

The western Pacific warm pool (WPWP) is the heat engine of the global climate system delivering vast amounts of heat and moisture to the atmosphere. Controls on regional convection, however, are numerous, making it difficult to simulate past and future changes in WPWP hydroclimate with confidence. Here, we synthesize new and previously available precipitation sensitive records from the WPWP spanning the last and present interglacial periods. We find two primary modes of rainfall variability, both driven by precession forcing, that are common to both interglacial periods: (a) a contraction of the tropical rain band across the interglacial and (b) a mid-interglacial strengthening of the Pacific Walker Circulation (PWC). We further demonstrate that while the amplitude of the change in seasonal insolation across the Holocene is far lower than during the LIG due to the low eccentricity state of Earth's orbit, the response of regional rainfall is comparable during both interglacials, indicating a nonlinear response to the insolation forcing. Finally, we suggest an enhanced sensitivity of the PWC to non-insolation climate forcing, including greenhouse gases and sea level change, under strongly reduced boreal fall insolation as observed during the late Holocene and late LIG.

Plain Language Summary

The western Pacific warm pool (WPWP) contains the warmest surface water in the global oceans and is therefore responsible for transferring large amounts of heat and moisture to the atmosphere and fueling high rates of rainfall. The intensity and distribution of this rainfall is modulated by complex interactions between regional monsoon systems and the cross-equator and equatorial Pacific zonal temperature gradients, which makes it difficult to assess how regional rainfall will respond to past and future climate change. In this paper, we produce a new record of rainfall from the WPWP spanning the last two warm periods in Earth history. We compare this new record to previously published reconstructions of rainfall from the WPWP. We find that variations in rainfall in the WPWP during warm periods are dominantly controlled by changes in the cross-equator contrast in incoming solar radiation driven by changes in orbital precession leading to two responses: (a) a north-south expansion and contraction and (b) an east-west shift in the region of maximum precipitation. These results provide insight to the sensitivity of rainfall in the western Pacific to climate forcing.

1. Introduction

The western Pacific warm pool (WPWP) is home to Earth's warmest surface ocean waters, fueling deep atmospheric convection that supplies vast amounts of latent heat and moisture to the atmosphere. Small perturbations in sea surface temperature (SST) influence the location and strength of convection in the rising limb of the Hadley and Walker circulations, perturbing planetary scale atmospheric circulation, atmospheric heating, and tropical hydrology (Neale & Slingo, 2003; H. Wang & Mehta, 2008). Variations in the regional moisture budget are responsible for flooding, landslides, droughts, and wildfires that impact the lives of the more than 300 million people living in Maritime Continent nations and the frequency, intensity, and impacts of these events are only expected to grow (Fortunato et al., 2022; Ghosh & Shepherd, 2023). Papua New Guinea (PNG) is among the most vulnerable and least resilient countries to climate change impacts (Chen et al., 2024). Major climate impacts include extreme heat, sea level rise, and extreme rain events leading to flooding and landslides, with large economic and human costs (Michael, 2019). Constraining future projections of tropical convection and rainfall in the region is therefore critical, but remains difficult to simulate with confidence due to the complex interactions between the Intertropical Convergence Zone (ITCZ), the South Pacific Convergence Zone (SPCZ), the Hadley and Walker circulation, and the seasonal strengthening of the Asian and Australian monsoon systems (De Deckker, 2016).

The ITCZ is a band of heavy rainfall and convection that migrates seasonally toward the warmer hemisphere in the tropics (Schneider et al., 2014). Observational records since the late 1970s and early 1980s indicate substantial regional variability, but an overall narrowing of the ITCZ coupled to an intensification of precipitation, particularly within the Pacific basin (Byrne et al., 2018; Wodzicki & Rapp, 2016; Zhou et al., 2011) Additionally, these same studies indicate no significant trend in the latitudinal location of the ITCZ across the same time periods. Looking to the future, a majority of models indicate continued contraction of the ITCZ (Byrne & Schneider, 2016; Byrne et al., 2018). Notably, weakening of the ITCZ does not necessarily imply a reduction in rainfall as precipitation intensity is regulated by both circulation and atmospheric moisture content (Seager et al., 2010). Projections of changes in ITCZ location exhibit much greater disagreement among models than metrics of width and strength (Byrne et al., 2018; McFarlane & Frierson, 2017). A recent study suggests potential for substantial zonal heterogeneity in the mean shift of the tropical rain belt, with southward shifts in the eastern Pacific and Atlantic sector, a northward shift across eastern Africa and the Indian Ocean, and possibly no shift in the western Pacific (Mamalakis et al., 2021). While this result remains to be tested, it suggests that regionally distinct responses of tropical rainfall to climate forcing must be considered when projecting into the future and the past.

In contrast, on orbital timescales the behavior of the ITCZ is largely considered globally coherent, moving north at precession minima when NH summer insolation peaks and south at precession maxima (Haug et al., 2001; Y. Wang et al., 2008). Convincing evidence of this behavior exists in most regions, though the phase relationship between the insolation forcing and the rainfall response is still debated (Clemens & Prell, 2007; Y. Wang et al., 2008). A recent compilation of Holocene precipitation-sensitive records, the interval with by far the greatest data coverage and spanning roughly half a precession cycle, confirms this behavior in the vast majority of the tropics and extratropical monsoon systems, though data are notably limited over the oceans and in the eastern and southern margins of the western tropical Pacific (Hancock et al., 2023). State-of-the-art climate models generally agree with proxy data and are particularly consistent within monsoon regions, especially the African, South American, and Indian Monsoon regions (Hancock et al., 2023). Model-model agreement and proxy-model agreement, however, are less consistent over the WPWP and associated monsoon systems to its north and south (Hancock et al., 2023), likely reflecting the complexity of regional controls on rainfall and convection.

Here, we present new reconstructions of runoff based on variations in marine sediment elemental ratios (Fe/Ca and Ti/Ca) obtained by X-Ray Fluorescence (XRF) core scanning and from reconstructions of surface ocean salinity, based on planktic foraminifer Mg/Ca & δ^{18}O. Our study focuses on the last and present interglacial periods at International Ocean Discovery Program Site U1485 recovered off the northern coast of Papua New Guinea in the heart of the WPWP (Figure 1). These new records are synthesized with previously published precipitation sensitive records from the central WPWP and its northern and southern margins to assess the primary modes of hydroclimate variability during the two most recent warm interglacial periods. During these periods, we find that the primary mode of hydroclimate variability within the WPWP and across the Maritime Continent reflects an expansion and contraction response of the ITCZ within the region that is distinct from the north to south migration observed in the EEP (e.g., Koutavas & Lynch-Stieglitz, 2004) and throughout the Northern and Southern hemisphere monsoon regions (Hancock et al., 2023 and refs within). The second mode is associated with the strength of tropical Pacific Walker circulation, which is also connected to pressure systems over the North Pacific. Moreover, we analyzed the time-slice Community Earth System Model (CESM 1.2) simulation results to further investigate these hydroclimate patterns.

2. Data and Methods

2.1. Holocene and Last Interglacial Precipitation History of Northern PNG

International Ocean Discovery Program (IODP) site U1485 (03°06.16′S, 142°47.59′E, 1145 m water depth) was collected during IODP Expedition 363 to the WPWP in 2016 (Rosenthal et al., 2018). Site U1485 is located ~19 km from the northern coast of PNG and ~200 km west of the Sepik and Ramu River mouths. The Sepik/Ramu river systems as well as a number of other tributaries along the island's northern coast supply terrigenous sediments in surface and near-bottom sediment plumes, largely bypassing the narrow (<2 km) continental shelf, and accumulating in deeper waters (Kineke et al., 2000; Milliman et al., 1999). The observed sedimentology

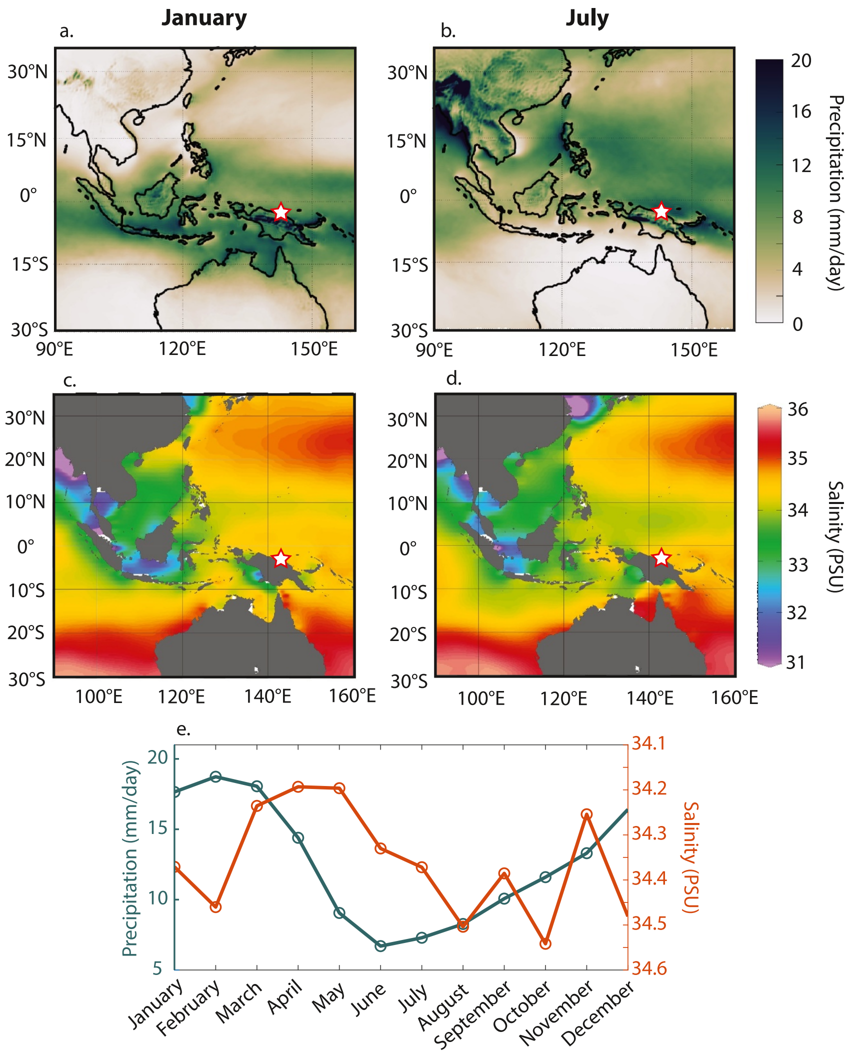

Figure 1. (a, b) Total precipitation from ERA5 monthly averaged data from 1950 to 2022, 0.25° lat × 0.25° long global grid in January (a) and July (b) (Hersbach et al., 2023). Location of IODP Site U1485 indicated with red and white star. (c, d) Sea surface salinity climatological mean from World Ocean Atlas 2023 (Reagan et al., 2024) and plotted using Ocean Data View for January (c) and July (d). (e) Monthly average daily precipitation rate (mm/day) (Hersbach et al., 2023) centered over the Sepik and Ramu River catchments (5°S, 143.75°E) in green plotted with the monthly average sea surface salinity (WOA23) in orange.

(Rosenthal et al., 2018) and documented high sedimentation rates at Site U1485 of 62 and 45 cm/ky for the Holocene and LIG are evidence of the substantial influx of these terrigenous sediments to the drill site (Bova et al., 2021). We recalibrated the planktic ^{14}C dates for Site U1485 published in Bova et al. (2021) to IntCal20 using the Undatable software package (Lougheed & Obrochta, 2019). IntCal20 is used in place of Marine20 because we are able to estimate local reservoir age variations using eight paired wood ^{14}C dates (Bova et al., 2021).

Variations in the terrigenous fraction of sediment cores recovered from the northern margin of PNG have been linked to changes in continental rainfall over Northern Papua New Guinea (N. PNG) (Aiello et al., 2019; Dang, Wu, et al., 2020; Tachikawa et al., 2011; J. Wu et al., 2013). We measured changes in the downcore contribution of terrigenous sediments at IODP site U1485 using ratios of elements characteristic of the terrigenous fraction (Ti, Fe, and K) to Ca, which reflects biogenic carbonates. We also employ a second, independent indicator of N. PNG rainfall: the surface ocean oxygen isotopic composition. The $\delta^{18}O_{sw}$ of the mixed layer is regulated by the freshwater flux, which at IODP site U1485 reflects both riverine discharge, and thus continental rainfall, as well as direct precipitation to the sea surface, in addition to secondary oceanographic factors, that is, horizontal and vertical advection and entrainment (Delcroix et al., 2014).

2.1.1. Downcore Variations in Bulk Sediment Geochemistry

We measured changes in the downcore contribution of terrigenous sediments at IODP site U1485 using a third-generation Avaatech X-ray fluorescence (XRF) core scanner at the IODP Gulf Coast Repository in College Station, Texas (USA). Measurements were taken every 2 cm along the shipboard splice across Holocene and LIG core sections. The archive core sections were gently scraped to remove the uppermost surface layer to provide a fresh, level surface and covered with a 4 μm thick Ultralene plastic film (SPEX Centriprep, Inc.) immediately prior to scanning to protect the detector. Scanning was performed using the generator settings of 9 kV, 250 μA, 6 s acquisition time, and no filter.

Following the best-practices outlined in Dunlea et al. (2020), we calibrated the XRF elemental intensities ratios against discrete quantitative major and minor element measurements from the same core depths. Eight Holocene bulk sediment samples were dissolved via flux fusion largely following the techniques described by Murray et al. (2000) and diluted to a final concentration of 1:1750 by mass. Solutions were analyzed for all 10 major and five trace elements, including Ba, Cr, Ni, Sr, and Zr, via inductively coupled plasma optical emission spectrometry (ICP-OES) at Rutgers University. Accuracy was determined by comparing the measured concentration of 4 reference standards, BCR-1 (basalt), JG-2 (granite), AGV-2 (andesite), and MAG-1 (marine mud) with their certified value and is expressed as a percentage of recovery (Rec %). Major elements (except Si) were quantified to within 5% of the accepted values, and all minor elements and Si to within 10%. A simple least squares linear regression was fit to the XRF elemental intensity and the quantitative element concentrations, both expressed as natural log ratios (Figure S1 in Supporting Information S1). The Pearson correlation coefficient (r^2) was greater than 0.9 for the three elemental ratios used here: Ti/Ca, Fe/Ca, and K/Ca, which indicates that intensity variations that arise from instrument aging or drift and/or inhomogeneities in the sediment core itself, that is, porosity, are effectively removed.

Following past work in the region (Tachikawa et al., 2011; J. Wu et al., 2013), the log ratios of Ti/Ca, Fe/Ca, and K/Ca are utilized to assess variations in the sediment terrigenous component at site U1485 through time. As nannofossils, benthic, and planktic foraminifers are a minor sedimentary component at Site U1485, with the $CaCO_3$ content ranging from 5% to 13% across the interglacials, variations in these ratios are dominated by changes in the terrigenous element contributions rather than variations in biogenic carbonate production. Furthermore, despite the potential for geochemical differentiation of the terrigenous fraction via weathering and transport processes and/or variable source regions, we find that the evolution of all three terrigenous elemental ratios are broadly indistinguishable in terms of trends and variability during the Holocene (Figure 2). Thus, the accumulation of coarse, refractory minerals, such as Ti-rich rutile and anatase, appears to track variations in the influx of clays and mafic minerals characterized by high K and Fe concentrations. Henceforth, we therefore use ln (Ti/Ca) to represent the downcore variations in the terrigenous component at IODP Site U1485.

2.1.2. Surface Ocean Freshwater Balance From the $\delta^{18}O$ of Seawater

The $\delta^{18}O$ of the planktic foraminifera *Globigerinoides ruber (sensu stricto)* (212–300 μm) was measured approximately every 10 cm over the upper 14.4 m CCSF-A (Holocene, Termination I, 0–20 ka) and approximately every 10 cm between 86.3 and 103.9 m CCSF-A (104–137 ka, LIG, Termination II). These data were measured at the same intervals as Mg/Ca datum from the same species and core previously published in Bova et al. (2021). An average of 14 individual foraminifera were gently cleaned in doubled distilled water and analyzed for $\delta^{18}O$ on a Micromass Optima stable isotope mass spectrometer with a multiprep device at Rutgers University. The long-term precision of the instrument is 0.08‰ for $\delta^{18}O$. Foraminifer preservation at IODP Site U1485 is excellent and glassy, with no evidence of dissolution, recrystallization or cementation (Rosenthal et al., 2017), thus no depth-related correction for salinity was applied.

Salinity was calculated using the Paleo-Seawater Uncertainty Solver version 2.1 for MATLAB (Thirumalai et al., 2016). This code uses a bootstrap Monte Carlo procedure to solve for seawater $\delta^{18}O$, salinity, and propagated uncertainty using foraminiferal Mg/Ca and $\delta^{18}O$ data. We apply the traditional multi-species Mg/Ca—temperature calibration from Anand et al. (2003). Note that the choice of calibration only makes a difference when assessing the absolute temperature, and has no significant impact on the calculated temperature anomalies, and

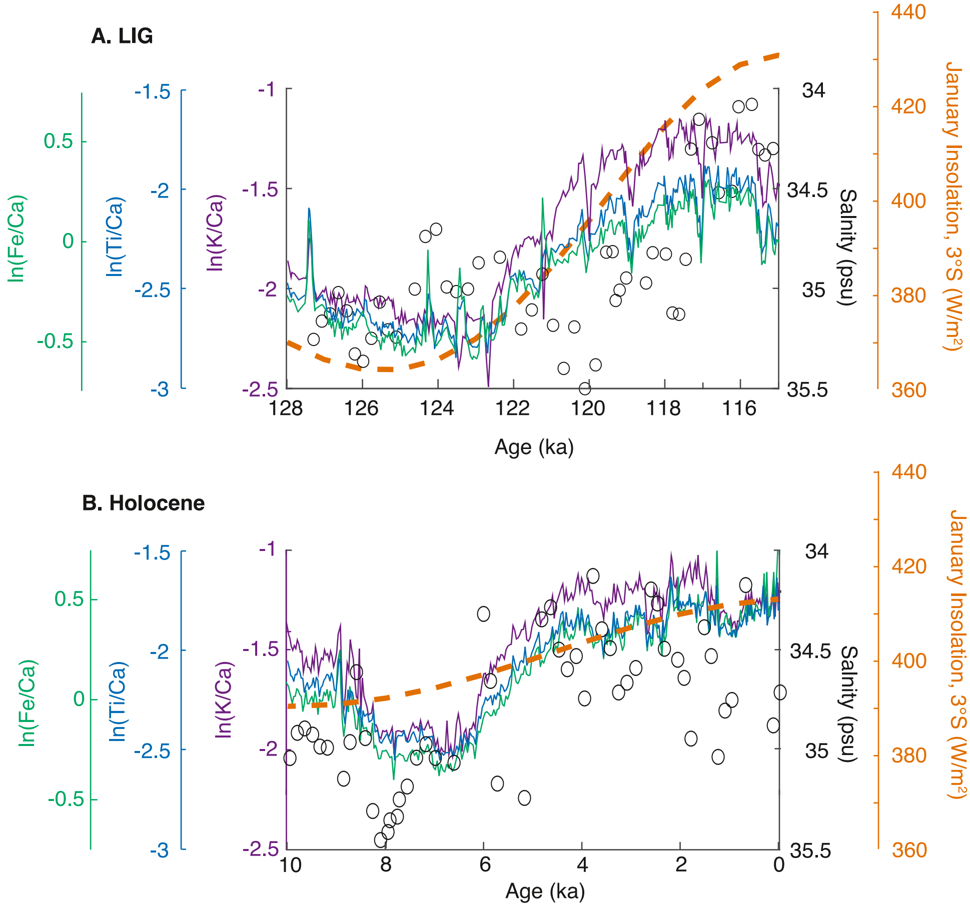

Figure 2. IODP Site U1485 ln(Ti/Ca) (blue), ln(Fe/Ca) (green), and ln(K/Ca) (purple) plotted with salinity (black open circles) estimated from *G. ruber ss* Mg/Ca and carbonate $\delta^{18}O$ using the Paleo-Seawater Uncertainty Solver version 2.1 for MATLAB (Thirumalai et al., 2016). (round symbols; (Bova et al., 2021)) and January insolation at 3°S (orange) (Huybers & Eisenman, 2006) for the LIG (A.) and Holocene (B.). The modern mean annual sea surface salinity at the nearest grid cell (2.5°S, 142.5°E) tracks seasonal changes in rainfall over N. PNG with a ~2 months lag (Figure 1) ranging from 34.5 in the "dry" season to 34.2 in the wet season (World Ocean Atlas 2023).

thus no significant impact on salinity anomalies (Bova et al., 2021; Rosenthal et al., 2022). In addition, we utilize the (Bemis et al., 1998) high light equation ($T = 14.9 - 4.8*(\delta^{18}O - \delta^{18}O_{sw} + 0.27)$) and the local salinity $- \delta^{18}O_{sw}$ relation from Hollstein et al. (2017) ($\delta^{18}O_{sw} = 0.37*\text{Salinity} - 12.4$). $\delta^{18}O_{sw}$ values were corrected for ice volume-related changes using the sea-level curve of Spratt and Lisiecki (2016) prior to conversion to salinity (Figure S2 in Supporting Information S1).

2.2. Climate Model Simulation

In this study, CESM1.2 time-slice simulations at preindustrial and 6 ka (Zhu & Poulsen, 2021) were utilized to investigate the changes in the tropical Pacific ITCZ and Walker circulation during the mid-Holocene. CESM1.2 is a fully coupled global climate model composed of atmosphere, ocean, sea ice, and land surface modules (Hurrell et al., 2013). The preindustrial control run employed climatic forcing fixed at 1850 values. The mid-Holocene simulation was conducted following the Paleoclimate Modeling Intercomparison Project version 4 (PMIP4) protocol, including orbital parameters, greenhouse gases concentration, ice sheets, and vegetation coverage (Otto-Bliesner et al., 2017). Aerosol emissions and solar constant were prescribed at their preindustrial levels. These simulations spanned a duration of 900 model years with atmosphere and land resolution of 1.9° × 2.25° and ocean resolution of ~1° (Zhu et al., 2017). For our analysis, we focused on the model output from the last 200 years to ensure that the system has reached quasi-equilibrium.

3. Results and Discussion

3.1. Evolution of Northern PNG Rainfall During the Last Two Interglacial Periods

Proxy indicators of continental (bulk sediment Ti/Ca) and marine rainfall and advection (sea surface salinity, SSS) both indicate a mid-interglacial period of relative dryness followed by an increase in rainfall across both interglacials in N. PNG (Figure 2), consistent with previous studies from the region that showed a tight relationship with local summer insolation and rainfall (Tachikawa et al., 2011). During the Holocene, SSS and the ln (Ti/Ca) track one another closely, exhibiting evidence of a minimum in precipitation driven runoff and erosion between 8 and 6 ka, followed by an abrupt transition, within ~1 ky, to wetter conditions. The consistency between the two proxies, provides high confidence in the Holocene record of freshwater balance in N. PNG, and also suggests that variations in continental rainfall were either the primary control on SSS at site U1485 and/or were highly correlated with variations in offshore precipitation during this period. The consistency between proxies, however, is not as strong during the LIG. Although both SSS and the ln(Ti/Ca) are consistent with an increase in rainfall across the interglacial, the timing of the transition to apparently wetter conditions is substantially offset between the two proxy records, occurring from ~120 to 117 ka in the SSS record, and ~123 to 118 ka in the record of ln(Ti/Ca) (Figure 2). The timing of this transition in the SSS data is not sensitive to the choice of sea level curve used to correct for ice volume (Figure S2 in Supporting Information S1). Rather, the discrepancy may be related to the different response times of the two proxies. While ln(Ti/Ca) data are point measurements, the foraminifer δ^{18}O and Mg/Ca were analyzed from shells within 2 cm intervals and therefore represent conditions spanning at least ~50 years. Differences in land versus sea precipitation and/or non-rainfall related variations in the seawater δ^{18}O signal related to variations in horizontal and vertical advection and entrainment may also contribute. Alternatively, the SSS is derived from seawater δ^{18}O signature measured on the planktic foraminifer *G. ruber ss*, which at this location disproportionately reflects surface ocean conditions during the NH summer/fall season (SH winter/spring) (Bova et al., 2021). In contrast, the ln(Ti/Ca) records the integrated yearly terrigenous flux, which together with its faster response time and more limited sensitivity to changing oceanographic conditions, leads us to consider this proxy as being more representative of the total annual precipitation budget during the LIG.

The observed increase in ln(Ti/Ca) at IODP site U1485 across the Holocene and last interglacial, is consistent with a minimum in summer insolation (3°S, January) that occurred at 125 and 10 ka, approximately in phase with the observed minima in ln(Ti/Ca) and inferred peak dryness during the LIG and preceding the Holocene minima in ln(Ti/Ca) by 2–3 ky. However, the magnitude of change in both the elemental and salinity data appears to be insensitive to the magnitude of change in incoming austral summer insolation. Holocene elemental ratios increase by ~0.75 and salinity decreases by ~1 psu. During the LIG, the magnitude of the change in elemental ratios and salinity is comparable to that observed during the Holocene despite austral summer insolation increasing by ~2.5x the increase during the Holocene. Millennial-scale variability is also detected during the Holocene and LIG in both proxy records. Due to (a) the substantial difference in sampling resolution, salinity data points were integrated across 2 cm about every 10 cm or ~150–250 years versus point measurements analyzed every 2 cm or ~30–50 years for the XRF ln(Ti/Ca) data, and (b) the smoothing that results from the PSU solver calculation, the millennial-scale variability is much more pronounced in the elemental scanning data.

At present, rainfall in N. PNG is dominantly regulated by three distinct, but related mechanisms: the position of the ITCZ, the seasonal strengthening of the Asian-Australian monsoon system, and the El Niño Southern Oscillation (ENSO) (De Deckker, 2016). Although PNG receives more than 100 cm of rainfall per month year-round, rainfall over the island reaches a maximum during SH summer, between January and April, when the ITCZ shifts southward and the Australian monsoon strengthens. Within the Sepik-Ramu basin, rainfall peaks at over 500 mm/month in February and decreases to a minimum of ~200 mm/month in June (Figure 1) (Hersbach et al., 2023), though there is substantial spatial variability due to orographic effects (Smith et al., 2013; Xie & Arkin, 1998). On interannual timescales, the rainfall in PNG varies with ENSO, decreasing over the western and southern parts of the country during El Niño events, particularly during the drier Austral winter period, but increasing in northeastern PNG (Smith et al., 2013). Finally, shifts in the position of the SPCZ, which are linked to both the position of the ITCZ and ENSO state, exert a more limited influence on rainfall totals in N. PNG, of just a few mm/day even across extreme swings (Cai et al., 2012).

Previous work links variation in PNG precipitation on multi-millennial timescales to precession-driven variations in the north-south position of the ITCZ, and secondarily to ENSO or ENSO-like modes (Tachikawa et al., 2011; Tierney et al., 2012). Our data are generally consistent with this interpretation, with evidence of drier conditions in

Table 1
Precipitation-Sensitive Proxy Records Included in Principal Components Analysis

Location	Archive	Proxy	Coverage	Reference
N. PNG, IODP site U1485 (03.103°S, 142.793°E)	Marine Sediment	XRF ln(Ti/Ca), $\delta^{18}O_{sw}$	Holocene and LIG	This study
NW Australia, IODP Site U1483 (13.087°S,121.804°E)	Marine Sediment	XRF ln(K/Ca)	Holocene and LIG	Zhang et al. (2020)
Borneo (4°N, 115°E)	Speleothem	$\delta^{18}O_{carb}$	Holocene and LIG	Carolin et al. (2013, 2016)
Hulu (32.5°N, 110.43°E), Sanbao (32.67°N, 110.43°E), and Dongge (25.28°N, 108.08°E) Cave, SE China	Speleothem	$\delta^{18}O_{carb}$	Holocene and LIG	Cheng et al. (2009, 2016), Dykoski et al. (2005), Kelly et al. (2006), Y. Wang et al. (2008); Y. J. Wang et al. (2001), Yuan et al. (2004)
Flores, Indonesia, Liang Luar Cave (8.533°S, 120.433°E)	Speleothem	$\delta^{18}O_{carb}$	Holocene only	Griffiths et al. (2009)
S. China, Huguangyan Maar Lake (21.15°N, 110.283°E)	Lake Sediment	Loss on Ignition	Holocene only	X. Wu et al. (2012)
NW Australia, cave KNI-51 (15.3°S, 128.62°E)	Speleothem	$\delta^{18}O_{carb}$	Holocene only	Denniston et al. (2013)
NW Australia, MD01-2378 (13.083°S, 121.788° E)	Marine Sediment	XRF ln(K/Ca)	Holocene only	Kuhnt et al. (2015)
NW Australia, SO185-18460 (8.790°S, 128.641°E)	Marine Sediment	XRF ln(K/Ca)	Holocene only	Kuhnt et al. (2015)
Offshore Sulawesi, Indonesia, BJ8-03-70GGC (3.566°S, 119.383°E)	Marine Sediment	δD_{wax}	Holocene only	Tierney et al. (2012)

N. PNG during the mid-Holocene (8–6 ka) and mid-LIG (125–121 ka), when summer insolation increases in the NH and the ITCZ is generally thought to be located further north. However, the transition from drier to wetter conditions during both interglacials is not a linear response to the insolation forcing, but occurs faster than the change in incoming austral summer insolation, particularly during the Holocene (Figure 2). Furthermore, data from PNG alone are not sufficient to diagnose the mechanism responsible for the observed variations in rainfall. For example, while N-S migration of the ITCZ is the dominant mode of variability on seasonal timescales, recent studies suggest that the dominant mode of variability in the W. Pacific ITCZ over recent millennia (Denniston et al., 2016; Konecky et al., 2013), during NH cooling events (Yang et al., 2023), and perhaps even on precession timescales (Singarayer et al., 2017; Zhang et al., 2020), was expansion and contraction, rather than north to south shifts. Fortunately, these various modes/drivers of rainfall variability give rise to distinct spatial patterns of rainfall across the WPWP that can be leveraged to differentiate between them.

3.2. A Regional Perspective

The proxy records from IODP Site U1485 provide a robust history of paleo-precipitation in N. PNG, recording a combination of continental and nearshore precipitation, but diagnosing the mechanism(s) responsible for the observed variations requires a regional perspective that can capture spatial patterns in paleo-hydrology. We therefore collated precipitation sensitive records from the heart of the WPWP as well as its northern and southern margins that span the last and current interglacial periods with <0.2 ky resolution ($n = 4$) (Text S1 in Supporting Information S1). We also included additional Holocene only records that span at least the period from 0.5 to 9 ka ($n = 6$). Proxy records included in this compilation are listed in Table 1.

To identify common modes of variability within the precipitation-sensitive data sets from the WPWP, we conducted a principal components analysis (PCA). Data were interpolated to a common timestep (0.2 ky) and each data set was normalized by calculating its z-score. Separate PCA analyses were conducted for the Holocene and LIG. As fewer records are available for the LIG, relative to the Holocene, we repeated the analysis for the Holocene using only records that contain a LIG section to ensure the results were comparable between the two interglacials and not biased by different spatial coverages. Results for the Holocene PC analysis with all records and with only records that also have a LIG section are similar (Figure S3, Table S3 in Supporting Information S1), which suggests the LIG analysis is not compromised substantively by the relative lack of available records.

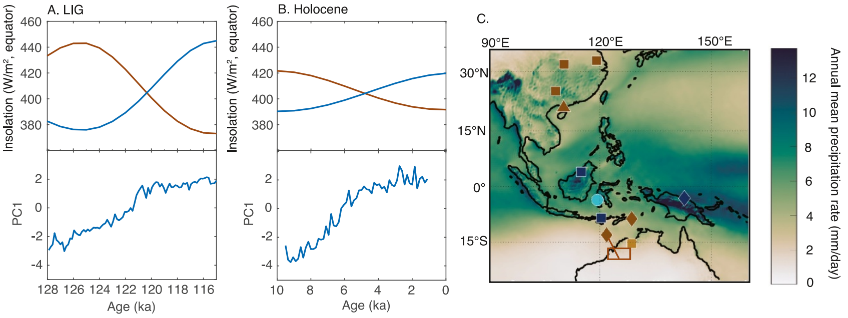

Figure 3. (a, b top panels) January (blue) and July (brown) insolation at the equator (bottom panels) PC 1 of the LIG (a) and Holocene (b) records listed in Table 1. (c) Annual mean precipitation rate from ERA5 monthly averaged data from 1950 to 2022 over the Western Pacific (Hersbach et al., 2023). Site locations and the sign of the loadings of PC1 at each site are indicated by the color of the location marker. Blue colors indicate a positive correlation with PC1 and brown a negative correlation (dark blue = positive loading (>0.2); light blue = positive loading >0.1; brown = negative loading ≤ −0.2; light brown = negative loading ≥ −0.2 & ≤ −0.1)). Symbol indicates the proxy record type (diamonds = XRF; squares = speleothem $\delta^{18}O_{carb}$; circle = δD_{wax}; triangle = loss on ignition. For sites with both a Holocene and LIG section the loading color markers are the same for both periods. For precise loading values see Supporting Information S1 (Tables S1 and S2 in Supporting Information S1). Brown box represents the Fitzroy River catchment, which dominates the runoff records from Site MD01-2378/IODP Site U1483. Colormap from Thyng et al. (2016).

3.2.1. PC1: Precession-Scale Expansion and Contraction of the ITCZ

The first principal component of both the Holocene and LIG analyses accounts for 49% and 69% of the variability in the data sets, respectively, and reflects the regional rainfall response to precession-scale variations in the interhemispheric temperature contrast (Figure 3). Yet, rather than observing anti-phased precipitation north and south of the equator consistent with north to south shifts in the mean position of the ITCZ, PC 1 yields negative loadings for all records on the northern and southern margins of the WPWP and positive loadings for near equatorial sites indicating an expansion and contraction response of the ITCZ to the precessional forcing (Figure 3, Tables S1 and S2 in Supporting Information S1). Additionally, in the early Holocene and early LIG we observe maximum rainfall in records located on the margins of the tropics and minimum rainfall within ∼10° of the equator indicating an expansion of the ITCZ, followed by a contraction of the ITCZ toward the equator in the later part of the interglacials.

Although an expansion and contraction response of the ITCZ has been proposed on millennial and sub-millennial timescales (Denniston et al., 2016; Konecky et al., 2013), fewer studies report this behavior on orbital timescales. Notably, an expansion and contraction response to precession forcing was recently proposed for the Indo-Pacific region (Zhang et al., 2020), with the addition of the first orbital-scale rainfall record from the southern margin of the ITCZ. Anti-phased precipitation records recovered from the northern margin of the ITCZ range (Cheng et al., 2009, 2016; Dykoski et al., 2005; Kelly et al., 2006; Y. J. Wang et al., 2001; Y. Wang et al., 2008; X. Wu et al., 2012; Yuan et al., 2004) and the central equatorial region of the WPWP (Carolin et al., 2013; Griffiths et al., 2009; Tierney et al., 2012) were previously interpreted to reflect north-south shifts in the position of the ITCZ, but the addition of this new record from the southern margin of the ITCZ suggests the conventional interpretation may not be correct. We emphasize, however, that our results do not preclude north-south shifts in the WPWP ITCZ from occurring. For example, the ITCZ may have shifted meridionally in response to North Atlantic cold events (e.g., Gibbons et al., 2014) and/or changes in land exposure (Zhang et al., 2020) during deglaciations, which would have had larger and more rapid impacts on the interhemispheric temperature gradient and land-sea moisture transport than precession forcing alone, though this is still debated (Yang et al., 2023).

Modeling studies are also mixed in the simulated response of the WPWP ITCZ to precession forcing, with some showing substantial north-south shifts in the ITCZ (Kutzbach et al., 2008), minor (<1°) variations in its mean latitudinal position (Donohoe et al., 2013; McGee et al., 2014), and, another, interhemispheric symmetric expansion and contraction over the oceans and antiphased north-south shifts over continents (Singarayer et al., 2017). Singarayer et al. (2017) demonstrate that over the oceans, the ITCZ is still responding to the interhemispheric temperature gradient, moving north in response to precession minima, when insolation and heating is greater in the northern hemisphere. Yet despite lower insolation in austral summer (boreal winter) south

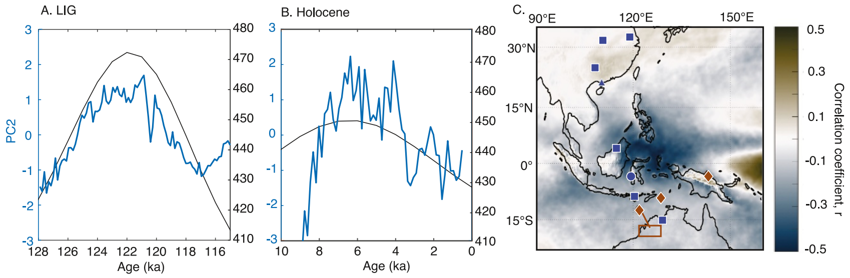

Figure 4. Evolution of PC2 (blue) during the LIG (a) and Holocene (b) plotted with September insolation (black) at the equator. (c) Spatial correlation of monthly rainfall from ERA5 monthly averaged data from 1950 to 2022 (Hersbach et al., 2023) with the NOAA/CPC monthly Nino 3.4 index from 1950 to 2022. Site locations and the sign of the loadings of PC2 at each site are indicated by the color of the location marker (dark blue = positive loading (>0.2); light blue = positive loading >0.1; brown = negative loading ≤ −0.2; light brown = negative loading ≥ −0.2 & ≤−0.1)). Symbol indicates the proxy record type (diamonds = XRF; squares = speleothem $\delta^{18}O_{carb}$; circle = δD_{wax}; triangle = loss on ignition. For loading values see Supporting Information S1 (Tables S1 and S2). For sites with both a Holocene and LIG section the loading color markers are the same for both periods. Symbol indicates the proxy record type (diamonds = XRF; squares = speleothem $\delta^{18}O_{carb}$; circle = δD_{wax}; triangle = loss on ignition. For precise loading values see Supporting Information S1 (Tables S1 and S2). Brown box represents the Fitzroy River catchment, which dominates the runoff records from Site MD01-2378/IODP Site U1483. Colormap from Thyng et al. (2016).

of the equator, insolation also decreases in the NH and, due to its greater land area, cooling is greater in the northern hemisphere than the southern hemisphere. As a result, during precession minima (as occurred in the early Holocene and mid-LIG) the ITCZ moves farther north in boreal summer and farther south in austral summer leading to an expansion of the ITCZ. Although the proxies in our compilation primarily reflect variations in rainfall over land in the WPWP, the mode of rain belt variation in the region displays oceanic character in the model (Singarayer et al., 2017) reflecting the maritime nature of regional climate dynamics.

3.2.2. PC2: Precession-Paced Shift in the Strength of the Pacific Walker Circulation

The second principal component of both the Holocene and LIG analyses accounts for 17% and 21% of the variability, respectively, with reduced precipitation over N. PNG and NE Australia and enhanced precipitation in the heart of the Maritime Continent. Although the observed spatial pattern is not directly analogous to modern rainfall anomalies observed during La Niña events of the last century, the evolution of PC2 tracks variations in equatorial September insolation (Figure 4), which has been linked to changes in the Pacific Walker Circulation (PWC) (Clement et al., 1999; Dang, Jian, et al., 2020; Tian et al., 2018). PWC strength is directly tied to the equatorial Pacific zonal temperature gradient, which is particularly sensitive to late summer/fall heating due to the off equatorial position of the eastern Pacific ITCZ at this time, driving wind field convergence in the west and divergence in the east and hence asymmetrical heating across the equatorial Pacific (Clement et al., 1999). Although our results indicate expansion of the ITCZ away from the equator during both boreal and austral summer in the western Pacific in the early Holocene and early LIG, possibly indicating the PWC would be sensitive to late summer/fall heating in both hemispheres, the eastern Pacific ITCZ, which is more important for controlling the cross-equatorial wind field, does not, only shifting off the equator in boreal summer and limiting the sensitivity of the PWC to one season: boreal summer/fall (Hancock et al., 2023; Koutavas & Lynch-Stieglitz, 2004). The equatorial Pacific zonal gradient is additionally tied to the meridional temperature gradient, with extratropical cooling associated with upwelling of colder subsurface water in the eastern equatorial Pacific and a stronger zonal gradient (Kang et al., 2020). On precession timescales, variations in the meridional temperature gradient were likely dominated by the changing extent of both Arctic and Antarctic sea ice (Lee et al., 2017).

The evolution of PC2 across the Holocene parallels records from the WPWP and more distal locations that have been dynamically linked to equatorial Pacific ENSO-like changes in the strength of the PWC (Figure 5). A compilation of thermocline water temperature (TWT) records from within Maritime Continent waters exhibits a warming peak around ~7 ka, consistent with a strengthened PWC at this time and strengthened convection and precipitation over the western and central parts of the warm pool region (Dang, Jian, et al., 2020; Dang et al., 2012; Rosenthal et al., 2013), but drier conditions in northeastern PNG. The records diverge in the early Holocene between 10 and 8 ka, but the early Holocene TWT peak at 10 ka is attributed to a distinct mechanism, unrelated to the PWC, that of strengthened advection of south Pacific mid-latitude waters via the shallow overturning circulation (Dang, Jian, et al., 2020).

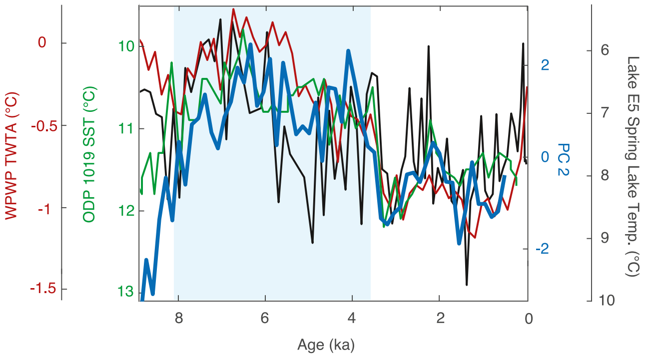

Figure 5. Holocene PC2 of the WPWP precipitation sensitive records plotted with records from the Pacific basin that are linked to variations in the Pacific Walker Circulation. (red) the mean Western Pacific thermocline temperature anomaly (Dang, Jian, et al., 2020) and (green) alkenone SST from central California coast at ODP Site 1019 (Barron & Anderson, 2011), and spring lake temperature from Lake E5 in northern Alaska (Longo et al., 2020).

PC2 also tracks Holocene proxy records sensitive to PWC changes at more distal locations, linked via teleconnections (Figure 5). For example, an enhanced PWC should correspond to cooler mean annual SSTs and reduced variance in the eastern equatorial Pacific and impact atmospheric features further afield in the North Pacific, that is, weakening and shifting the Aleutian Low westward, and strengthening and shifting the North Pacific High further north. Individual foraminiferal analyses confirm reduced variance in mid-Holocene SSTs in the EEP and traditional analyses record mean annual cooling in the region between ~6 and 4 ka, consistent with enhanced PWC at this time (Koutavas et al., 2006; Koutavas & Joanides, 2012). Shifting atmospheric features cannot be observed directly, but the impact of Rossby waves that propagate these changes from the tropics, lead to temperature, precipitation, and wind anomalies along the west coast of North America and northern Alaska. These are observed, most notably as widespread dry conditions in the southwestern U.S. (Benson et al., 2002; Palmer et al., 2023; Shuman et al., 2009), enhanced wind-driven upwelling leading to cooler SSTs off California (Barron & Anderson, 2011), and reduced lake temperatures in Alaska (Longo et al., 2020). The latter two indices are shown in Figure 5 and demonstrate the tight link between PC2 and other PWC sensitive records.

During the LIG, PC2 exhibits similar timing to the Holocene record, peaking in the mid-LIG in-phase with rising September insolation at the equator. PC2 also accounts for a comparable amount of variability within the data sets, ~20%, and exhibits the same spatial pattern among factor loadings (Figure 4b, Tables S1 and S2 in Supporting Information S1). Thus, although equivalent records of Holocene TWT from the WPWP and those from teleconnected regions are not available for the LIG, we conclude that PC2 from the LIG period reflects the same mechanism: PWC strength changes. Given the synchronicity of PWC variability to September insolation during both time intervals, our results support prior work tying the PWC to precession via phase locking with the seasonal cycle (Clement et al., 1999; Koutavas & Joanides, 2012).

In contrast to past studies (Chiang et al., 2022; Clement et al., 1999; Kaboth-Bahr & Mudelsee, 2022; Rustic et al., 2020), we found that the intensity range of the PWC is insensitive to variations in the amplitude of the seasonal cycle of insolation (Figure 4). An intensification in the PWC, as inferred from the zonal Pacific SST gradient at ~2.4 Ma was cautiously related to a period of low eccentricity and exceptionally muted precession amplitudes (Kaboth-Bahr & Mudelsee, 2022). Further, a modeling study indicated a change in the behavior of ENSO events in response to eccentricity, most notably a reduction in the mean event amplitude and a change in the coherence of cold (La Nina; strong PWC) and warm (El Nino, weak PWC) events under low eccentricity conditions (Clement et al., 1999). Yet, we found that during the LIG, when seasonality in incoming solar insolation was enhanced relative to the Holocene due to the higher eccentricity state of Earth's orbit, the observed modes of variability and their amplitude are comparable between the two interglacial periods (Figure 4). Disagreements in the sensitivity of the PWC to the amplitude of seasonal insolation forcing among studies may be attributed to the different indicators of PWC utilized (precipitation vs. SST gradients), timescales, and approaches employed (data vs. model) and should be explored further in the future.

Despite the discussed similarity, there is one notable distinction between the Holocene and LIG evolution of PC2 in our reconstructions: the nature of the transition from strong to weak PWC (Figure 4). While the PWC strength appears to follow variations in September insolation more or less directly during the LIG, the Holocene PWC exhibits a threshold response to the drop in September insolation at ~4 ka (Figure 4). A non-linear response to insolation decline in the mid-Holocene is detected elsewhere in the climate system, including, most famously, in the termination of the Green Sahara at ~5.5 ka (de Menocal et al., 2000; Tierney et al., 2017). A growing body of literature suggests the vegetation-dust climate feedbacks from the Sahara drying had a global footprint, impacting the behavior of the Asian and South American monsoon systems (Griffiths et al., 2009; Kaboth-Bahr et al., 2021; Tabor et al., 2020; Tiwari et al., 2023; Wolf et al., 2023) as well as the PWC (Griffiths et al., 2020; Pausata et al., 2017). Observations indicate that similar drying of a Green Sahara likely occurred during the LIG

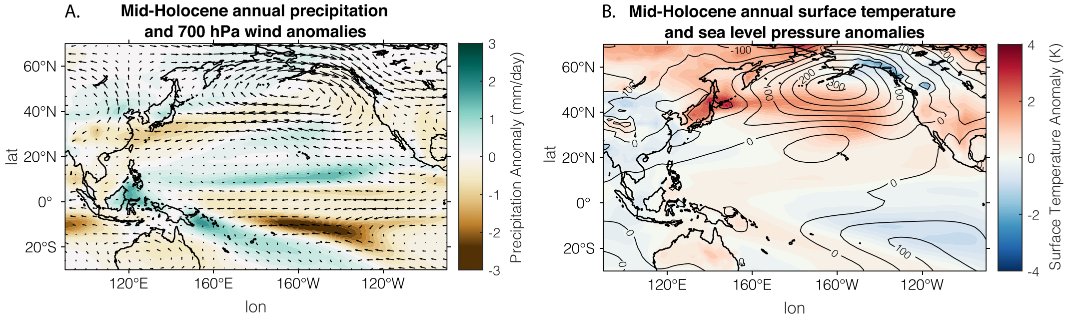

Figure 6. Simulated mid-Holocene anomalies (6 ka minus PI) in (a) annual precipitation and wind, and (b) annual surface temperature and sea level pressure in CESM 1.2.

(Kowalski et al., 1989; Osborne et al., 2008). Although proxy data are not available to directly constrain the rate of this transition, a modeling study suggests termination of the Green Sahara at the LIG was even more abrupt than during the Holocene (Li et al., 2022). Given the lack of an abrupt response in our PWC reconstruction it is therefore possible that the PWC response to the Holocene insolation decline was synchronous with, but independent from Saharan vegetation change. Alternatively, drying of the LIG Green Sahara may have proceeded more gradually than during the Holocene.

The Holocene is distinct from the LIG in two main ways that could have impacted the susceptibility of the PWC, and perhaps other components of the climate system such as Saharan vegetation, to abrupt change. First, as noted earlier, seasonality in incoming solar insolation was strongly reduced in the Holocene relative to the LIG. Although the range of PWC strength appears to be insensitive to the amplitude of the incoming seasonal insolation forcing (Figures 4a and 4b), its propensity to experience abrupt strength changes could nevertheless be impacted. Additionally or alternatively, changes in Holocene greenhouse gases (Bereiter et al., 2015), ice volume, and thus sea level far exceed that of the LIG, even considering the range of available LIG sea level curves (Figure S4 in Supporting Information S1) (Clark et al., 2020; Grant et al., 2012; Lambeck et al., 2014; Spratt & Lisiecki, 2016; Waelbroeck et al., 2002). While it is well documented that the Sunda Shelf was flooded by ~9.5 ky (Hanebuth et al., 2011; Linsley et al., 2010), and all Holocene sea level reconstructions indicate a reduction in the rate of sea level rise at roughly 6 ka (Figure S4 in Supporting Information S1), well before the transition from strong to weak PWC at 4 ka, some sea level reconstructions do indicate continued sea level rise across the mid- to late Holocene (Grant et al., 2012; Spratt & Lisiecki, 2016). Furthermore, paleo-shoreline reconstructions indicate a regional high stand in the West Pacific at 4.2 ka (Hanebuth et al., 2011). While determining the precise cause of the abrupt shift in the Holocene PWC is beyond the scope of this study, prior work has demonstrated the sensitivity of regional moisture balance and the PWC to changes in sea level and greenhouse gases (DiNezio & Tierney, 2013; Griffiths et al., 2009; Power & Kociuba, 2011), Saharan vegetation change (Pausata et al., 2017), and suggest that one or all could have contributed to the abrupt shift in PWC strength when insolation played a lesser role.

3.3. Model Simulations

We employed CESM 1.2 time-slice simulations to further investigate changes in ITCZ and PWC during the mid-Holocene, as indicated by our compilation of regional proxy records. Over the WPWP region, the simulated precipitation pattern is inhomogeneous, and we do not observe the expansion pattern of the tropical rain belt as indicated by our regional proxy compilation (Figure 6). In the WPWP, wetter condition is simulated over the central Maritime Continent and western equatorial Pacific, along with dryer condition over the northern and southern edges of the tropics, including Thailand, Vietnam, southeast China, as well as Java and northern Australia. The discrepancy between the ITCZ-related pattern in mid-Holocene hydroclimate proxy records and CESM 1.2 simulation over the WPWP could be attributed to several factors. These may include the intricate interactions between the ITCZ, Asian-Australian monsoon system, and PWC, as well as the complex topographical features of this region. It is worth noting that previous research on Holocene proxy and model comparisons based on PMIP simulations, has also suggested a relatively wide cross-model spread and low data-model agreement over the WPWP (Ackerley et al., 2017; Hancock et al., 2023). This underscores the complexities associated with understanding the dynamics of ITCZ in the WPWP region and the need for a more comprehensive spatial coverage of proxy records in this region.

Moreover, the mid-Holocene simulation exhibits stronger Walker circulation over the tropical Pacific relative to the preindustrial condition (6 ka minus PI) (Figure 6). This is characterized by cooler SST along with high sea level pressure over the central and eastern equatorial Pacific, accompanied by stronger easterly trade wind. The increased precipitation observed over northern Borneo and Sulawesi in the simulation aligns with the PC2 of our regional proxy records compilation. The intensified PWC and La Nina-like conditions contribute to stronger convection and precipitation over the western tropical Pacific. Furthermore, the higher sea level pressure and the presence of an anomalous anticyclone over the northeastern Pacific suggest a weaker Aleutian Low. This significant large-scale connection between the stronger PWC and weaker Aleutian Low during mid-Holocene is also indicated by proxy records. These include hydroclimate records from western North America (Du et al., 2021; Hermann et al., 2018), SST reconstructions off coastal California and Alaska (Barron & Anderson, 2011; Longo et al., 2020), as well as atmospheric circulation records from the central North Pacific (Bailey et al., 2018).

4. Future Lessons

Although models generally agree that the ITCZ will contract under future climate change, there is a high degree of uncertainty in constraining zonal shifts in its position (multimodel mean of −0.5 ± 1.2°N; (McFarlane & Frierson, 2017)). Convergence does arise among models, however, for zonal shifts within some longitudinal sectors, with more than ¾ of the 27 CMIP6 models suggesting a southward shift of the ITCZ in the eastern Pacific-Atlantic and a northward shift across eastern Africa and the Indian Ocean (Mamalakis et al., 2021). There is less agreement within the WPWP and the Maritime Continent, though the multimodel mean suggests no shift in the ITCZ zonal position in the annual mean due to symmetric decreases in the seasonal ITCZ migration. Although the timescale and forcing are distinct, our results are consistent with expansion-contraction as a primary mode of ITCZ variability in the WPWP region. Locally, our results support a “wet-gets-wetter” scenario within the WPWP, with increasing rainfall totals along the equator in the WPWP that will likely exacerbate local hazards associated with extreme rain events, such as flooding and landslides.

Our results further demonstrate that the strength of the PWC is sensitive to precession driven changes in boreal fall heating, consistent with previous studies (Clement et al., 1999; Dang, Jian, et al., 2020; Tian et al., 2018). Comparing and contrasting the evolution of the PWC during the Holocene and LIG, however, provides additional insight. We show a lack of sensitivity of the amplitude of PWC strength changes to the magnitude of change in maximum to minimum boreal fall insolation. Yet despite this insensitivity to the amplitude of change, we suggest that under strongly reduced boreal fall insolation levels and/or reduced seasonality, the PWC becomes increasingly sensitive to other climate forcings, which led to a non-linear response to insolation, resulting in an abrupt, rather than gradual, decrease in PWC strength in the late Holocene. The different response during the Holocene and LIG suggests that the abrupt response is possibly related to rising greenhouse gases and sea level. At present, we continue to experience reduced seasonality and boreal fall insolation, which suggests the PWC will maintain a heightened sensitivity to rising greenhouse house gas levels and resulting climate feedbacks into the future.

Data Availability Statement

The new data from IODP Site U1485, including downcore XRF geochemical data, planktic foraminifer δ^{18}O, and the updated Holocene chronology from that published previously in Bova et al. (2021) as well as a synthesis of all previously published data sets included in our analysis (Table 1) are archived in the Paleoclimatology Database supported by the National Centers for Environmental Information (Bova et al., 2025).

Acknowledgments
This research used samples and data provided by the International Ocean Discovery Program (IODP). We thank the science party, technical staff, and crew of IODP Expedition 363, who together ensured the successful recovery of IODP Site U1485 by the JOIDES Resolution. Funding was provided by NSF Grant P2C2-2432287 to X. Du, OCE-1834208 to Y. Rosenthal, and IODP USSSP Post Expedition Awards and OCE- 2202818 to S. C. Bova and Y. Rosenthal.

References

Ackerley, D., Reeves, J., Barr, C., Bostock, H., Fitzsimmons, K., Fletcher, M. S., et al. (2017). Evaluation of PMIP2 and PMIP3 simulations of mid-Holocene climate in the Indo-Pacific, Australasian and Southern Ocean regions. *Climate of the Past*, *13*(11), 1661–1684. https://doi.org/10.5194/cp-13-1661-2017

Aiello, I. W., Bova, S. C., Holbourn, A. E., Kulhanek, D. K., Ravelo, A. C., & Rosenthal, Y. (2019). Climate, sea level and tectonic controls on sediment discharge from the Sepik River, Papua New Guinea during the Mid- to Late Pleistocene. *Marine Geology*, *415*, 105954. https://doi.org/10.1016/j.margeo.2019.05.013

Anand, P., Elderfield, H., & Conte, M. H. (2003). Calibration of Mg/Ca thermometry in planktonic foraminifera from a sediment trap time series. *Paleoceanography*, *18*(2). https://doi.org/10.1029/2002PA000846

Bailey, H. L., Kaufman, D. S., Sloane, H. J., Hubbard, A. L., Henderson, A. C. G., Leng, M. J., et al. (2018). Holocene atmospheric circulation in the central North Pacific: A new terrestrial diatom and δ18O dataset from the Aleutian Islands. *Quaternary Science Reviews*, *194*, 27–38. https://doi.org/10.1016/j.quascirev.2018.06.027

Barron, J. A., & Anderson, L. (2011). Enhanced late Holocene ENSO/PDO expression along the margins of the eastern North Pacific. *Quaternary International*, *235*(1), 3–12. https://doi.org/10.1016/j.quaint.2010.02.026

Bemis, B. E., Spero, H. J., Bijma, J., & Lea, D. W. (1998). Reevaluation of the oxygen isotopic composition of planktonic foraminifera: Experimental results and revised paleotemperature equations. *Paleoceanography*, *13*(2), 150–160. https://doi.org/10.1029/98pa00070

Benson, L., Kashgarian, M., Rye, R., Lund, S., Paillet, F., Smoot, J., et al. (2002). Holocene multidecadal and multicentennial droughts affecting Northern California and Nevada. *Quaternary Science Reviews*, *21*(4), 659–682. https://doi.org/10.1016/S0277-3791(01)00048-8

Bereiter, B., Eggleston, S., Schmitt, J., Nehrbass-Ahles, C., Stocker, T. F., Fischer, H., et al. (2015). Revision of the EPICA Dome C CO_2 record from 800 to 600 kyr before present. *Geophysical Research Letters*, *42*(2), 542–549. https://doi.org/10.1002/2014GL061957

Bova, S. C., Rosenthal, Y., Liu, Z., Godad, S. P., & Yan, M. (2021). Seasonal origin of the thermal maxima at the Holocene and the last interglacial. *Nature*, *589*(7843), 548–553. https://doi.org/10.1038/s41586-020-03155-x

Bova, S. C., Rosenthal, Y., & Du, X. (2025). NOAA/WDS Paleoclimatology—Western Pacific Warm Pool (WPWP) Precipitation Sensitive Records from the Holocene and the Last Interglacial (LIG) [Dataset]. *NOAA National Centers for Environmental Information, Paleoclimatology Database*. https://doi.org/10.25921/27xk-d813

Byrne, M. P., Pendergrass, A. G., Rapp, A. D., & Wodzicki, K. R. (2018). Response of the intertropical convergence zone to climate change: Location, width, and strength. *Current Climate Change Reports*, *4*(4), 355–370. https://doi.org/10.1007/s40641-018-0110-5

Byrne, M. P., & Schneider, T. (2016). Narrowing of the ITCZ in a warming climate: Physical mechanisms. *Geophysical Research Letters*, *43*(21), 11350–11357. https://doi.org/10.1002/2016gl070396

Cai, W., Lengaigne, M., Borlace, S., Collins, M., Cowan, T., McPhaden, M. J., et al. (2012). More extreme swings of the South Pacific convergence zone due to greenhouse warming. *Nature*, *488*(7411), 365–369. https://doi.org/10.1038/nature11358

Carolin, S. A., Cobb, K. M., Lynch-Stieglitz, J., Moerman, J. W., Partin, J. W., Lejau, S., et al. (2016). Northern Borneo stalagmite records reveal West Pacific hydroclimate across MIS 5 and 6. *Earth and Planetary Science Letters*, *439*, 182–193. https://doi.org/10.1016/j.epsl.2016.01.028

Carolin, S. A., Cobb Kim, M., Adkins Jess, F., Clark, B., Conroy Jessica, L., Lejau, S., et al. (2013). Varied response of Western Pacific hydrology to climate forcings over the last glacial period. *Science*, *340*(6140), 1564–1566. https://doi.org/10.1126/science.1233797

Chen, C., Nobel, I., Hellmann, J., Coffee, J. M. M., & Chawla, N. (2024). University of Notre Dame global Adaptation index country index technical report.

Cheng, H., Edwards, R. L., Broecker, W. S., Denton, G. H., Kong, X., Wang, Y., et al. (2009). Ice age terminations. *Science*, *326*(5950), 248–252. https://doi.org/10.1126/science.1177840

Cheng, H., Edwards, R. L., Sinha, A., Spötl, C., Yi, L., Chen, S., et al. (2016). The Asian monsoon over the past 640,000 years and ice age terminations. *Nature*, *534*(7609), 640–646. https://doi.org/10.1038/nature18591

Chiang, J. C. H., Atwood, A. R., Vimont, D. J., Nicknish, P. A., Roberts, W. H. G., Tabor, C. R., & Broccoli, A. J. (2022). Two annual cycles of the Pacific cold tongue under orbital precession. *Nature*, *611*(7935), 295–300. https://doi.org/10.1038/s41586-022-05240-9

Clark, P. U., He, F., Golledge, N. R., Mitrovica, J. X., Dutton, A., Hoffman, J. S., & Dendy, S. (2020). Oceanic forcing of penultimate deglacial and last interglacial sea-level rise. *Nature*, *577*(7792), 660–664. https://doi.org/10.1038/s41586-020-1931-7

Clemens, S. C., & Prell, W. L. (2007). The timing of orbital-scale Indian monsoon changes. *Quaternary Science Reviews*, *26*(3), 275–278. https://doi.org/10.1016/j.quascirev.2006.11.010

Clement, A. C., Seager, R., & Cane, M. A. (1999). Orbital controls on the El Niño/Southern Oscillation and the tropical climate. *Paleoceanography*, *14*(4), 441–456. https://doi.org/10.1029/1999PA900013

Dang, H., Jian, Z., Bassinot, F., Qiao, P., & Cheng, X. (2012). Decoupled Holocene variability in surface and thermocline water temperatures of the Indo-Pacific Warm Pool. *Geophysical Research Letters*, *39*(1). https://doi.org/10.1029/2011GL050154

Dang, H., Jian, Z., Wang, Y., Mohtadi, M., Rosenthal, Y., Ye, L., et al. (2020). Pacific warm pool subsurface heat sequestration modulated Walker circulation and ENSO activity during the Holocene. *Science Advances*, *6*(42), eabc0402. https://doi.org/10.1126/sciadv.abc0402

Dang, H., Wu, J., Xiong, Z., Qiao, P., Li, T., & Jian, Z. (2020). Orbital and sea-level changes regulate the iron-associated sediment supplies from Papua New Guinea to the equatorial Pacific. *Quaternary Science Reviews*, *239*, 106361. https://doi.org/10.1016/j.quascirev.2020.106361

De Deckker, P. (2016). The Indo-Pacific warm pool: Critical to world oceanography and world climate. *Geoscience Letters*, *3*(1), 20. https://doi.org/10.1186/s40562-016-0054-3

Delcroix, T., Radenac, M.-H., Cravatte, S., Alory, G., Gourdeau, L., Léger, F., et al. (2014). Sea surface temperature and salinity seasonal changes in the western Solomon and Bismarck Seas. *Journal of Geophysical Research: Oceans*, *119*(4), 2642–2657. https://doi.org/10.1002/2013JC009733

de Menocal, P., Ortiz, J., Guilderson, T., Adkins, J., Sarnthein, M., Baker, L., & Yarusinsky, M. (2000). Abrupt onset and termination of the African humid period: Rapid climate responses to gradual insolation forcing. *Quaternary Science Reviews*, *19*(1), 347–361. https://doi.org/10.1016/S0277-3791(99)00081-5

Denniston, R. F., Ummenhofer, C. C., Wanamaker, A. D., Lachniet, M. S., Villarini, G., Asmerom, Y., et al. (2016). Expansion and contraction of the Indo-Pacific tropical rain belt over the last three millennia. *Scientific Reports*, *6*(1), 34485. https://doi.org/10.1038/srep34485

Denniston, R. F., Wyrwoll, K.-H., Polyak, V. J., Brown, J. R., Asmerom, Y., Wanamaker, A. D., et al. (2013). A Stalagmite record of Holocene Indonesian–Australian summer monsoon variability from the Australian tropics. *Quaternary Science Reviews*, *78*, 155–168. https://doi.org/10.1016/j.quascirev.2013.08.004

DiNezio, P. N., & Tierney, J. E. (2013). The effect of sea level on glacial Indo-Pacific climate. *Nature Geoscience*, *6*(6), 485–491. https://doi.org/10.1038/ngeo1823

Donohoe, A., Marshall, J., Ferreira, D., & Mcgee, D. (2013). The relationship between ITCZ location and cross-equatorial atmospheric heat transport: From the seasonal cycle to the last glacial maximum. *Journal of Climate*, *26*(11), 3597–3618. https://doi.org/10.1175/JCLI-D-12-00467.1

Du, X., Hendy, I., Hinnov, L., Brown, E., Zhu, J., & Poulsen, C. J. (2021). High-resolution interannual precipitation reconstruction of Southern California: Implications for Holocene ENSO evolution. *Earth and Planetary Science Letters*, *554*, 116670. https://doi.org/10.1016/j.epsl.2020.116670

Dunlea, A. G., Murray, R. W., Tada, R., Alvarez-Zarikian, C. A., Anderson, C. H., Gilli, A., et al. (2020). Intercomparison of XRF core scanning results from seven labs and approaches to practical calibration. *Geochemistry, Geophysics, Geosystems*, *21*(9), e2020GC009248. https://doi.org/10.1029/2020GC009248

Dykoski, C. A., Edwards, R. L., Cheng, H., Yuan, D., Cai, Y., Zhang, M., et al. (2005). A high-resolution, absolute-dated Holocene and deglacial Asian monsoon record from Dongge Cave, China. *Earth and Planetary Science Letters*, *233*(1), 71–86. https://doi.org/10.1016/j.epsl.2005.01.036

Fortunato, A., Herwartz, H., López, R. E., & Figueroa B, E. (2022). Carbon dioxide atmospheric concentration and hydrometeorological disasters. *Natural Hazards*, *112*(1), 57–74. https://doi.org/10.1007/s11069-021-05172-z

Ghosh, R., & Shepherd, T. G. (2023). Storylines of Maritime Continent dry period precipitation changes under global warming. *Environmental Research Letters*, *18*(3), 034017. https://doi.org/10.1088/1748-9326/acb788

Gibbons, F. T., Oppo, D. W., Mohtadi, M., Rosenthal, Y., Cheng, J., Liu, Z., & Linsley, B. K. (2014). Deglacial δ^{18}O and hydrologic variability in the tropical Pacific and Indian Oceans. *Earth and Planetary Science Letters*, *387*, 240–251. https://doi.org/10.1016/j.epsl.2013.11.032

Grant, K. M., Rohling, E. J., Bar-Matthews, M., Ayalon, A., Medina-Elizalde, M., Ramsey, C. B., et al. (2012). Rapid coupling between ice volume and polar temperature over the past 150,000 years. *Nature*, *491*(7426), 744–747. https://doi.org/10.1038/nature11593

Griffiths, M. L., Drysdale, R. N., Gagan, M. K., Zhao, J. X., Ayliffe, L. K., Hellstrom, J. C., et al. (2009). Increasing Australian–Indonesian monsoon rainfall linked to early Holocene sea-level rise. *Nature Geoscience*, *2*(9), 636–639. https://doi.org/10.1038/ngeo605

Griffiths, M. L., Johnson, K. R., Pausata, F. S. R., White, J. C., Henderson, G. M., Wood, C. T., et al. (2020). End of Green Sahara amplified mid- to late Holocene megadroughts in mainland Southeast Asia. *Nature Communications*, *11*(1), 4204. https://doi.org/10.1038/s41467-020-17927-6

Hancock, C. L., McKay, N. P., Erb, M. P., Kaufman, D. S., Routson, C. R., Ivanovic, R. F., et al. (2023). Global synthesis of regional holocene hydroclimate variability using proxy and model data. *Paleoceanography and Paleoclimatology*, *38*(6), e2022PA004597. https://doi.org/10.1029/2022PA004597

Hanebuth, T. J. J., Voris, H. K., Yokoyama, Y., Saito, Y., & Okuno, J. I. (2011). Formation and fate of sedimentary depocentres on Southeast Asia's Sunda Shelf over the past sea-level cycle and biogeographic implications. *Earth-Science Reviews*, *104*(1), 92–110. https://doi.org/10.1016/j.earscirev.2010.09.006

Haug, G. H., Hughen, K. A., Sigman, D. M., Peterson, L. C., & Röhl, U. (2001). Southward migration of the intertropical convergence zone through the holocene. *Science*, *293*(5533), 1304–1308. https://doi.org/10.1126/science.1059725

Hermann, N. W., Oster, J. L., & Ibarra, D. E. (2018). Spatial patterns and driving mechanisms of mid-holocene hydroclimate in western North America. *Journal of Quaternary Science*, *33*(4), 421–434. https://doi.org/10.1002/jqs.3023

Hersbach, H., Bell, B., Berrisford, P., Biavati, G., Horanyi, A., Mnoz Sabater, J., et al. (2023). ERA5 monthly averaged data on single levels from 1940 to present. https://doi.org/10.24381/cds.f17050d7

Hollstein, M., Mohtadi, M., Rosenthal, Y., Moffa Sanchez, P., Oppo, D., Martínez Méndez, G., et al. (2017). Stable oxygen isotopes and Mg/Ca in planktic foraminifera from modern surface sediments of the Western Pacific warm pool: Implications for thermocline reconstructions. *Paleoceanography*, *32*(11), 1174–1194. https://doi.org/10.1002/2017PA003122

Hurrell, J. W., Holland, M. M., Gent, P. R., Ghan, S., Kay, J. E., Kushner, P. J., et al. (2013). The Community Earth system model: A framework for collaborative research. *Bulletin of the American Meteorological Society*, *94*(9), 1339–1360. https://doi.org/10.1175/BAMS-D-12-00121.1

Huybers, P., & Eisenman, I. (2006). Integrated summer insolation % calculations. In *NOAA/NCDC paleoclimatology program data contribution (2006–079)*.

Kaboth-Bahr, S., Bahr, A., Zeeden, C., Yamoah, K. A., Lone, M. A., Chuang, C.-K., et al. (2021). A tale of shifting relations: East Asian summer and winter monsoon variability during the Holocene. *Scientific Reports*, *11*(1), 6938. https://doi.org/10.1038/s41598-021-85444-7

Kaboth-Bahr, S., & Mudelsee, M. (2022). The multifaceted history of the Walker Circulation during the Plio-Pleistocene. *Quaternary Science Reviews*, *286*, 107529. https://doi.org/10.1016/j.quascirev.2022.107529

Kang, S. M., Xie, S.-P., Shin, Y., Kim, H., Hwang, Y.-T., Stuecker, M. F., et al. (2020). Walker circulation response to extratropical radiative forcing. *Science Advances*, *6*(47), eabd3021. https://doi.org/10.1126/sciadv.abd3021

Kelly, M. J., Edwards, R. L., Cheng, H., Yuan, D., Cai, Y., Zhang, M., et al. (2006). High resolution characterization of the Asian Monsoon between 146,000 and 99,000 years B.P. from Dongge Cave, China and global correlation of events surrounding Termination II. *Palaeogeography, Palaeoclimatology, Palaeoecology*, *236*(1), 20–38. https://doi.org/10.1016/j.palaeo.2005.11.042

Kineke, G. C., Woolfe, K. J., Kuehl, S. A., Milliman, J. D., Dellapenna, T. M., & Purdon, R. G. (2000). Sediment export from the Sepik River, Papua New Guinea: Evidence for a divergent sediment plume. *Continental Shelf Research*, *20*(16), 2239–2266. https://doi.org/10.1016/S0278-4343(00)00069-8

Konecky, B. L., Russell, J. M., Rodysill, J. R., Vuille, M., Bijaksana, S., & Huang, Y. (2013). Intensification of southwestern Indonesian rainfall over the past millennium. *Geophysical Research Letters*, *40*(2), 386–391. https://doi.org/10.1029/2012GL054331

Koutavas, A., de Menocal, P. B., Olive, G. C., & Lynch-Stieglitz, J. (2006). Mid-Holocene El Niño–Southern Oscillation (ENSO) attenuation revealed by individual foraminifera in eastern tropical Pacific sediments. *Geology*, *34*(12), 993–996. https://doi.org/10.1130/g22810a.1

Koutavas, A., & Joanides, S. (2012). El Niño–Southern Oscillation extrema in the holocene and last glacial maximum. *Paleoceanography*, *27*(4). https://doi.org/10.1029/2012PA002378

Koutavas, A., & Lynch-Stieglitz, J. (2004). Variability of the marine ITCZ over the eastern Pacific during the past 30,000 years: Regional perspective and global context. In *The Hadley circulation: Present, past and future* (pp. 347–369). Springer.

Kowalski, K., Neer, W. V., Bocheński, Z., Młynarski, M., Rzebik-Kowalska, B., Szyndlar, Z., et al. (1989). A last interglacial Fauna from the Eastern Sahara. *Quaternary Research*, *32*(3), 335–341. https://doi.org/10.1016/0033-5894(89)90099-9

Kuhnt, W., Holbourn, A., Xu, J., Opdyke, B., De Deckker, P., Röhl, U., & Mudelsee, M. (2015). Southern Hemisphere control on Australian monsoon variability during the late deglaciation and Holocene. *Nature Communications*, *6*(1), 5916. https://doi.org/10.1038/ncomms6916

Kutzbach, J. E., Liu, X., Liu, Z., & Chen, G. (2008). Simulation of the evolutionary response of global summer monsoons to orbital forcing over the past 280,000 years. *Climate Dynamics*, *30*(6), 567–579. https://doi.org/10.1007/s00382-007-0308-z

Lambeck, K., Rouby, H., Purcell, A., & Sambridge, M. (2014). Sea level and global ice volumes from the last glacial maximum to the holocene. *Proceedings of the National Academy of Sciences of the United States of America*, *111*(43), 15296–15303. https://doi.org/10.1073/pnas.1411762111

Lee, J.-E., Shen, A., Fox-Kemper, B., & Ming, Y. (2017). Hemispheric sea ice distribution sets the glacial tempo. *Geophysical Research Letters*, *44*(2), 1008–1014. https://doi.org/10.1002/2016GL071307

Li, H., Renssen, H., & Roche, D. M. (2022). Comparison of the green-to-desert Sahara transitions between the Holocene and the last interglacial. *Climate of the Past*, *18*(10), 2303–2319. https://doi.org/10.5194/cp-18-2303-2022

Linsley, B. K., Rosenthal, Y., & Oppo, D. W. (2010). Holocene evolution of the Indonesian throughflow and the western Pacific warm pool. *Nature Geoscience*, *3*(8), 578–583. https://doi.org/10.1038/ngeo920

Longo, W. M., Huang, Y., Russell, J. M., Morrill, C., Daniels, W. C., Giblin, A. E., & Crowther, J. (2020). Insolation and greenhouse gases drove Holocene winter and spring warming in Arctic Alaska. *Quaternary Science Reviews*, *242*, 106438. https://doi.org/10.1016/j.quascirev.2020.106438

Lougheed, B. C., & Obrochta, S. P. (2019). A rapid, deterministic age-depth modeling routine for geological sequences with Inherent depth uncertainty. *Paleoceanography and Paleoclimatology*, *34*(1), 122–133. https://doi.org/10.1029/2018PA003457

Mamalakis, A., Randerson, J. T., Yu, J.-Y., Pritchard, M. S., Magnusdottir, G., Smyth, P., et al. (2021). Zonally contrasting shifts of the tropical rain belt in response to climate change. *Nature Climate Change*, *11*(2), 143–151. https://doi.org/10.1038/s41558-020-00963-x

McFarlane, A. A., & Frierson, D. M. W. (2017). The role of ocean fluxes and radiative forcings in determining tropical rainfall shifts in RCP8.5 simulations. *Geophysical Research Letters*, *44*(16), 8656–8664. https://doi.org/10.1002/2017GL074473

McGee, D., Donohoe, A., Marshall, J., & Ferreira, D. (2014). Changes in ITCZ location and cross-equatorial heat transport at the last glacial maximum, Heinrich Stadial 1, and the mid-Holocene. *Earth and Planetary Science Letters*, *390*, 69–79. https://doi.org/10.1016/j.epsl.2013.12.043

Michael, P. S. (2019). Current evidence and future projections: A Comparative analysis of the impacts of climate change on critical climate-sensitive areas of Papua New Guinea. *SAINS TANAH - Journal of Soil Science and Agroclimatology*, *16*(2), 25. [Agriculture; Climate change; Critical impact areas; PNG; Precipitation; Temperature]. https://doi.org/10.20961/stjssa.v16i2.35712

Milliman, J. D., Farnsworth, K. L., & Albertin, C. S. (1999). Flux and fate of fluvial sediments leaving large islands in the East Indies. *Journal of Sea Research*, *41*(1), 97–107. https://doi.org/10.1016/S1385-1101(98)00040-9

Murray, R., Miller, D. J., & Kryc, K. (2000). Analysis of major and trace elements in rocks, sediments, and interstitial waters by inductively coupled plasma–atomic emission spectrometry (ICP-AES).

Neale, R., & Slingo, J. (2003). The maritime continent and its role in the global climate: A GCM study. *Journal of Climate*, *16*(5), 834–848. https://doi.org/10.1175/1520-0442(2003)016<0834:TMCAIR>2.0.CO;2

Osborne, A. H., Vance, D., Rohling, E. J., Barton, N., Rogerson, M., & Fello, N. (2008). A humid corridor across the Sahara for the migration of early modern humans out of Africa 120,000 years ago. *Proceedings of the National Academy of Sciences of the United States of America*, *105*(43), 16444–16447. https://doi.org/10.1073/pnas.0804472105

Otto-Bliesner, B. L., Braconnot, P., Harrison, S. P., Lunt, D. J., Abe-Ouchi, A., Albani, S., et al. (2017). The PMIP4 contribution to CMIP6—Part 2: Two interglacials, scientific objective and experimental design for Holocene and Last Interglacial simulations. *Geoscientific Model Development*, *10*(11), 3979–4003. https://doi.org/10.5194/gmd-10-3979-2017

Palmer, H. M., Vriesman, V. P., Livsey, C. M., Fish, C. R., & Hill, T. M. (2023). Holocene climate and oceanography of the coastal Western United States and California current system. *Climate of the Past*, *19*(1), 199–232. https://doi.org/10.5194/cp-19-199-2023

Pausata, F. S. R., Zhang, Q., Muschitiello, F., Lu, Z., Chafik, L., Niedermeyer, E. M., et al. (2017). Greening of the Sahara suppressed ENSO activity during the mid-Holocene. *Nature Communications*, *8*(1), 16020. https://doi.org/10.1038/ncomms16020

Power, S. B., & Kociuba, G. (2011). The impact of global warming on the Southern Oscillation Index. *Climate Dynamics*, *37*(9), 1745–1754. https://doi.org/10.1007/s00382-010-0951-7

Reagan, J. R., Boyer, T. P., García, H. E., Locarnini, R. A., Baranova, O. K., Bouchard, C., et al. (2024). *World Ocean Atlas 2023*. NOAA National Centers for Environmental Information. Dataset. NCEI Accession 0270533.

Rosenthal, Y., Bova, S., & Zhou, X. (2022). A user guide for choosing planktic foraminiferal Mg/Ca-temperature calibration. *Paleoceanography and Paleoclimatology*, *37*(6), e2022PA004413. https://doi.org/10.1029/2022PA004413

Rosenthal, Y., Holbourn, A. E., Kulhanek, D. K., & Scientists, E. (2017). *Expedition 363 preliminary report: Western Pacific warm pool*. I. O. D. Program.

Rosenthal, Y., Holbourn, A. E., Kulhanek, D. K., & Scientists, E. (2018). Western Pacific Warm Pool. In *Proceedings of the International Ocean Discovery Program* (Vol. 363).

Rosenthal, Y., Linsley, B. K., & Oppo, D. W. (2013). Pacific Ocean heat content during the past 10,000 years. *Science*, *342*(6158), 617–621. https://doi.org/10.1126/science.1240837

Rustic, G. T., Polissar, P. J., Ravelo, A. C., & White, S. M. (2020). Modulation of late Pleistocene ENSO strength by the tropical Pacific thermocline. *Nature Communications*, *11*(1), 5377. https://doi.org/10.1038/s41467-020-19161-6

Schneider, T., Bischoff, T., & Haug, G. H. (2014). Migrations and dynamics of the intertropical convergence zone. *Nature*, *513*(7516), 45–53. https://doi.org/10.1038/nature13636

Seager, R., Naik, N., & Vecchi, G. A. (2010). Thermodynamic and dynamic mechanisms for large-scale changes in the hydrological cycle in response to global warming. *Journal of Climate*, *23*(17), 4651–4668. https://doi.org/10.1175/2010jcli3655.1

Shuman, B., Henderson, A. K., Colman, S. M., Stone, J. R., Fritz, S. C., Stevens, L. R., et al. (2009). Holocene lake-level trends in the Rocky Mountains, U.S.A. *Quaternary Science Reviews*, *28*(19), 1861–1879. https://doi.org/10.1016/j.quascirev.2009.03.003

Singarayer, J. S., Valdes, P. J., & Roberts, W. H. G. (2017). Ocean dominated expansion and contraction of the late Quaternary tropical rainbelt. *Scientific Reports*, *7*(1), 9382. https://doi.org/10.1038/s41598-017-09816-8

Smith, I., Moise, A., Inape, K., Murphy, B., Colman, R., Power, S., & Chung, C. (2013). ENSO-related rainfall changes over the New Guinea region. *Journal of Geophysical Research: Atmospheres*, *118*(19), 10665–10675. https://doi.org/10.1002/jgrd.50818

Spratt, R. M., & Lisiecki, L. E. (2016). A Late Pleistocene sea level stack. *Climate of the Past*, *12*(4), 1079–1092. https://doi.org/10.5194/cp-12-1079-2016

Tabor, C., Otto-Bliesner, B., & Liu, Z. (2020). Speleothems of South American and Asian Monsoons Influenced by a Green Sahara. *Geophysical Research Letters*, *47*(22), e2020GL089695. https://doi.org/10.1029/2020GL089695

Tachikawa, K., Cartapanis, O., Vidal, L., Beaufort, L., Barlyaeva, T., & Bard, E. (2011). The precession phase of hydrological variability in the Western Pacific Warm Pool during the past 400 ka. *Quaternary Science Reviews*, *30*(25), 3716–3727. https://doi.org/10.1016/j.quascirev.2011.09.016

Thirumalai, K., Quinn, T. M., & Marino, G. (2016). Constraining past seawater δ18O and temperature records developed from foraminiferal geochemistry. *Paleoceanography*, *31*(10), 1409–1422. https://doi.org/10.1002/2016PA002970

Thyng, K. M., Greene, C. A., Hetland, R. D., Zimmerle, H. M., & DiMarco, S. F. (2016). True colors of oceanography: Guidelines for effective and accurate colormap selection. *Oceanography*, *29*(3), 9–13. https://doi.org/10.5670/oceanog.2016.66

Tian, Z., Li, T., & Jiang, D. (2018). Strengthening and Westward Shift of the Tropical Pacific Walker Circulation during the Mid-Holocene: PMIP Simulation Results. *Journal of Climate*, *31*(6), 2283–2298. https://doi.org/10.1175/JCLI-D-16-0744.1

Tierney, J. E., Oppo, D. W., LeGrande, A. N., Huang, Y., Rosenthal, Y., & Linsley, B. K. (2012). The influence of Indian Ocean atmospheric circulation on Warm Pool hydroclimate during the Holocene epoch. *Journal of Geophysical Research*, *117*(D19). https://doi.org/10.1029/2012JD018060

Tierney, J. E., Pausata, F. S. R., & de Menocal, P. B. (2017). Rainfall regimes of the Green Sahara. *Science Advances*, *3*(1), e1601503. https://doi.org/10.1126/sciadv.1601503

Tiwari, S., Ramos, R. D., Pausata, F. S. R., LeGrande, A. N., Griffiths, M. L., Beltrami, H., et al. (2023). On the Remote Impacts of Mid-Holocene Saharan Vegetation on South American Hydroclimate: A Modeling Intercomparison. *Geophysical Research Letters*, *50*(12), e2022GL101974. https://doi.org/10.1029/2022GL101974

Waelbroeck, C., Labeyrie, L., Michel, E., Duplessy, J.-C., Mcmanus, J. F., Lambeck, K., et al. (2002). Sea-level and deep water temperature changes derived from benthic foraminifera isotopic records. *Quaternary Science Reviews*, *21*(1–3), 295–305. https://doi.org/10.1016/s0277-3791(01)00101-9

Wang, H., & Mehta, V. M. (2008). Decadal Variability of the Indo-Pacific Warm Pool and Its Association with Atmospheric and Oceanic Variability in the NCEP–NCAR and SODA Reanalyses. *Journal of Climate*, *21*(21), 5545–5565. https://doi.org/10.1175/2008JCLI2049.1

Wang, Y., Cheng, H., Edwards, R. L., Kong, X., Shao, X., Chen, S., et al. (2008). Millennial- and orbital-scale changes in the East Asian monsoon over the past 224,000 years. *Nature*, *451*(7182), 1090–1093. https://doi.org/10.1038/nature06692

Wang, Y. J., Cheng, H., Edwards, R. L., An, Z. S., Wu, J. Y., Shen, C. C., & Dorale, J. A. (2001). A High-Resolution Absolute-Dated Late Pleistocene Monsoon Record from Hulu Cave, China. *Science*, *294*(5550), 2345–2348. https://doi.org/10.1126/science.1064618

Wodzicki, K., & Rapp, A. (2016). Long-term characterization of the Pacific ITCZ using TRMM, GPCP, and ERA-Interim. *Journal of Geophysical Research: Atmospheres*, *121*(7), 3153–3170. https://doi.org/10.1002/2015jd024458

Wolf, A., Ersek, V., Braun, T., French, A. D., McGee, D., Bernasconi, S. M., et al. (2023). Deciphering local and regional hydroclimate resolves contradicting evidence on the Asian monsoon evolution. *Nature Communications*, *14*(1), 5697. https://doi.org/10.1038/s41467-023-41373-9

Wu, J., Liu, Z., & Zhou, C. (2013). Provenance and supply of Fe-enriched terrigenous sediments in the western equatorial Pacific and their relation to precipitation variations during the late Quaternary. *Global and Planetary Change*, *108*, 56–71. https://doi.org/10.1016/j.gloplacha.2013.06.002

Wu, X., Zhang, Z., Xu, X., & Shen, J. (2012). Asian summer monsoonal variations during the Holocene revealed by Huguangyan maar lake sediment record. *Palaeogeography, Palaeoclimatology, Palaeoecology*, *323–325*, 13–21. https://doi.org/10.1016/j.palaeo.2012.01.020

Xie, P., & Arkin, P. A. (1998). Global monthly precipitation estimates from satellite-observed outgoing longwave radiation. *Journal of Climate*, *11*(2), 137–164. https://doi.org/10.1175/1520-0442(1998)011<0137:GMPEFS>2.0.CO;2

Yang, Y., Zhang, L., Yi, L., Zhong, F., Lu, Z., Wan, S., et al. (2023). A contracting intertropical convergence zone during the Early Heinrich Stadial 1. *Nature Communications*, *14*(1), 4695. https://doi.org/10.1038/s41467-023-40377-9

Yuan, D., Cheng, H., Edwards, R. L., Dykoski Carolyn, A., Kelly Megan, J., Zhang, M., et al. (2004). Timing, duration, and transitions of the last interglacial Asian Monsoon. *Science*, *304*(5670), 575–578. https://doi.org/10.1126/science.1091220

Zhang, P., Xu, J., Holbourn, A., Kuhnt, W., Beil, S., Li, T., et al. (2020). Indo-Pacific hydroclimate in response to changes of the intertropical convergence zone: Discrepancy on precession and obliquity bands over the last 410 kyr. *Journal of Geophysical Research: Atmospheres*, *125*(14), e2019JD032125. https://doi.org/10.1029/2019JD032125

Zhou, Y., Xu, K. M., Sud, Y., & Betts, A. (2011). Recent trends of the tropical hydrological cycle inferred from Global Precipitation Climatology Project and International Satellite Cloud Climatology Project data. *Journal of Geophysical Research*, *116*(D9), D09101. https://doi.org/10.1029/2010jd015197

Zhu, J., Liu, Z., Brady, E., Otto-Bliesner, B., Zhang, J., Noone, D., et al. (2017). Reduced ENSO variability at the LGM revealed by an isotope-enabled Earth system model. *Geophysical Research Letters*, *44*(13), 6984–6992. https://doi.org/10.1002/2017GL073406

Zhu, J., & Poulsen, C. J. (2021). Last Glacial Maximum (LGM) climate forcing and ocean dynamical feedback and their implications for estimating climate sensitivity. *Climate of the Past*, *17*(1), 253–267. https://doi.org/10.5194/cp-17-253-2021